RadioGraphics

Radionuclide Bone Imaging: An Illustrative Review[1]

Charito Love, MD • Anabella S. Din, MD • Maria B. Tomas, MD
Tomy P. Kalapparambath, MD • Christopher J. Palestro, MD

Bone scintigraphy with technetium-99m–labeled diphosphonates is one of the most frequently performed of all radionuclide procedures. Radionuclide bone imaging is not specific, but its excellent sensitivity makes it useful in screening for many pathologic conditions. Moreover, some conditions that are not clearly depicted on anatomic images can be diagnosed with bone scintigraphy. Bone metastases usually appear as multiple foci of increased activity, although they occasionally manifest as areas of decreased uptake. Traumatic processes can often be detected, even when radiographic findings are negative. Most fractures are scintigraphically detectable within 24 hours, although in elderly patients with osteopenia, further imaging at a later time is sometimes indicated. Athletic individuals are prone to musculoskeletal trauma, and radionuclide bone imaging is useful for identifying pathologic conditions such as plantar fasciitis, stress fractures, "shin splints," and spondylolysis, for which radiographs may be nondiagnostic. A combination of focal hyperperfusion, focal hyperemia, and focally increased bone uptake is virtually diagnostic for osteomyelitis in patients with nonviolated bone. Bone scintigraphy is also useful for evaluating disease extent in Paget disease and for localizing avascular necrosis in patients with negative radiographs. Radionuclide bone imaging will likely remain a popular and important imaging modality for years to come.

Index terms: Bone neoplasms, secondary, 40.33 • Bones, infection, 40.21 • Bones, radionuclide studies, 40.1216, 40.12172 • Radionuclide imaging, 40.1216, 40.12172 • Reflex sympathetic dystrophy, 40.565 • Spondylolysis, 30.42 • Trauma, 40.41

RadioGraphics 2003; 23:341–358 • **Published online** 10.1148/rg.232025103

[1]From the Division of Nuclear Medicine, Long Island Jewish Medical Center, 270-05 76th Ave, New Hyde Park, NY 11040. Presented as an education exhibit at the 2001 RSNA scientific assembly. Received May 28, 2002; revision requested July 24 and received August 19; accepted August 19. **Address correspondence to** C.L. (e-mail: *love@lij.edu*).

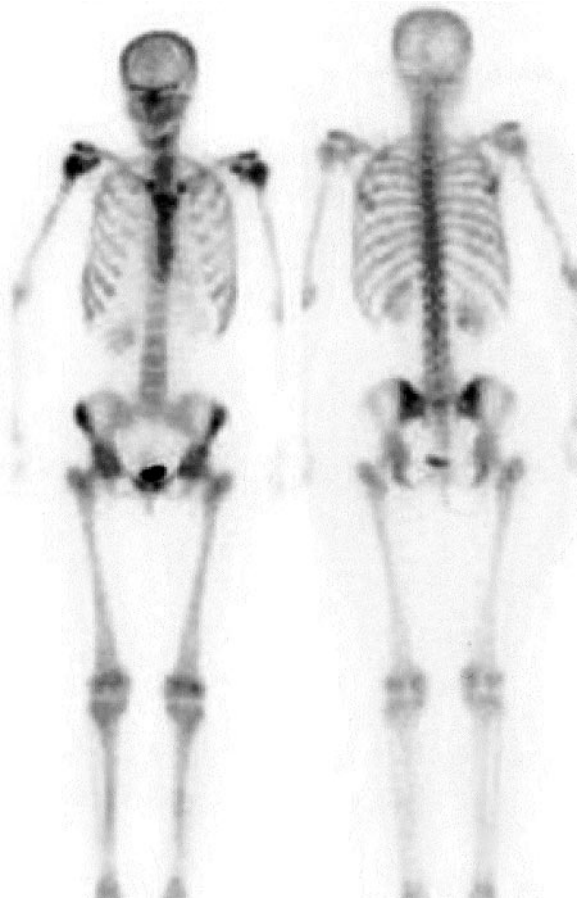

Figure 1. Anterior (left) and posterior (right) whole-body bone scintigrams obtained in an adult demonstrate normal anatomy.

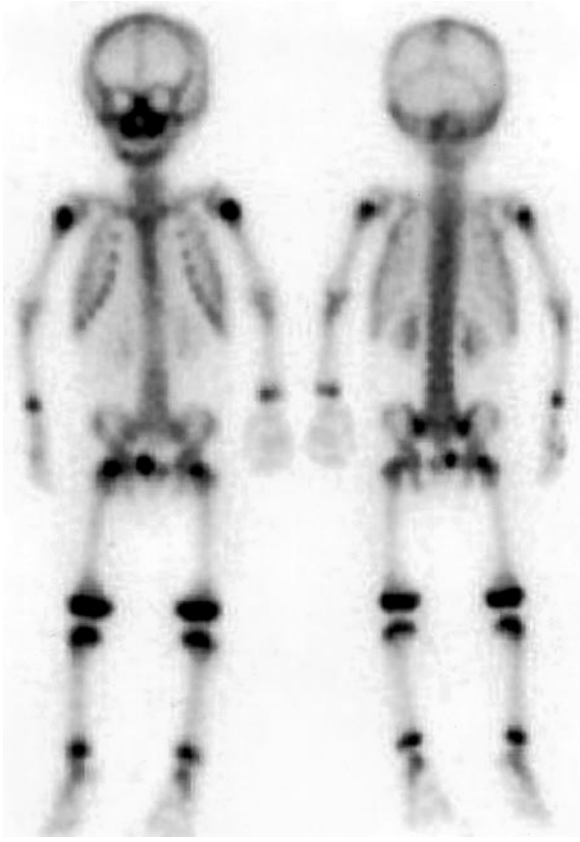

Figure 2. Anterior (left) and posterior (right) whole-body bone scintigrams obtained in a child demonstrate normal anatomy. Note the increased activity in the physes of the long bones and in the hematopoietically active facial bones.

Introduction

Bone scintigraphy is one of the most frequently performed of all radionuclide procedures. Radionuclide bone imaging is quick, relatively inexpensive, widely available, and exquisitely sensitive and is invaluable in the diagnostic evaluation of numerous pathologic conditions. The procedure is performed with technetium-99m–labeled diphosphonates. These compounds accumulate rapidly in bone, and by 2–6 hours after injection, about 50% of the injected dose is in the skeletal system. The uptake mechanisms of diphosphonates have not been completely elucidated. Presumably they are adsorbed to the mineral phase of bone, with relatively little binding to the organic phase. The degree of radiotracer uptake depends primarily on two factors: blood flow and, perhaps more importantly, the rate of new bone formation (1–3).

Although protocols vary among institutions, imaging is typically performed 2–6 hours after intravenous administration of 740–925 MBq (20–25 mCi) of Tc-99m–labeled diphosphonates. The delay between injection and imaging allows clearance of the radiotracer from the soft tissues, resulting in a higher target-to-background ratio and improved visualization of bone. Skeletal detail can be further enhanced by encouraging patients to drink copious amounts of fluid after radiotracer injection. A gamma camera equipped with a low-energy, high-resolution collimator will

a. b.

Figure 3. **(a)** Anterior bone scintigram shows discrete focal activity in the left maxilla (arrowhead) due to a dental process and heart-shaped activity in the anterior neck (arrow) representing the thyroid cartilage, both of which are normal variants. **(b)** Posterior bone scintigram shows focal activity in the right side of the neck (arrow) caused by a cervical osteophyte.

yield the highest-resolution images. Additional anterior and posterior whole-body images are often obtained as needed.

In this article, we discuss and illustrate normal bone scintigraphic findings as well as findings in metastatic disease, trauma, infection, and miscellaneous conditions (Paget disease, hypertrophic osteoarthropathy, reflex sympathetic dystrophy, avascular necrosis, spondylolysis, venous obstruction, extraosseous activity, artifacts).

Normal Scintigraphic Findings

There is symmetric distribution of activity throughout the skeletal system in healthy adults. Urinary bladder activity, faint renal activity, and minimal soft-tissue activity are also normally present (Fig 1) (3). In children, intense symmetric uptake in the physes of the long bones, which represent centers of normal growth and hematopoietic production, is typically present. The marrow-containing flat facial bones also demonstrate accumulation of radiotracer in children (Fig 2) (3).

The accumulation of radiotracer in bone generally decreases with age (3). However, there are sites of persistently increased symmetric uptake, such as the acromial and coracoid processes of the scapulae, the medial ends of the clavicles, the junction of the body and manubrium of the sternum (angle of Louis), and the sacral alae. Increased radiotracer accumulation in the jaw may be due to dental disease or to malocclusion of dentures. Symmetric areas of increased calvarial activity occurs in hyperostosis frontalis. In the neck, activity in calcified thyroid cartilage and in the apophyseal joints of the cervical vertebrae in patients with asymptomatic degenerative changes can also be seen (Fig 3) (3).

Metastatic Disease

Many if not most bone scans are performed in patients with a diagnosis of malignancy, especially carcinoma of the breast, prostate gland, and lung. Radionuclide bone imaging plays an integral part in tumor staging and management. This modality is extremely sensitive for detecting skeletal abnormalities, and numerous studies have confirmed that it is considerably more sensitive than conventional radiography for this purpose (4–7). About 75% of patients with malignancy and pain have abnormal bone scintigraphic findings. Perhaps even more importantly, 25%–45% of asymptomatic patients with malignancy have scintigraphic evidence of bone metastases. The usual pattern consists of increased radiotracer deposition in areas of osteoblastic reparative activity in response to tumor osteolysis (7–9). The presence of multiple, randomly distributed areas of increased uptake of varying size, shape, and intensity is highly suggestive of bone metastases (Fig 4). Although multiple foci of increased activity may be

encountered in other pathologic conditions, it is often possible to distinguish metastatic disease from other entities by analyzing the pattern of distribution of the abnormalities. Traumatic injury, in contrast to metastatic disease, generally manifests as discrete focal abnormalities of similar intensity. Multifocal rib trauma has a characteristic linear distribution. In patients with osteoporosis, kyphosis and an H-shaped sacral fracture suggest the correct diagnosis (Fig 5). In older patients, osteoarthritis and degenerative changes may manifest as areas of intense activity on radionuclide bone images. These changes can be distinguished from metastatic disease by virtue of their characteristic location (eg, knees, hands, wrists). Involvement of both sides of the joint is common in arthritis but unusual in malignant conditions (10).

When the metastatic process is diffuse, virtually all of the radiotracer is concentrated in the skeleton, with little or no activity in the soft tissues or urinary tract. The resulting pattern, which is characterized by excellent bone detail, is frequently referred to as a superscan (Fig 6) (9–11). A superscan may also be associated with metabolic bone disease. Unlike in metastatic disease, however, the uptake in metabolic bone disease is more uniform in appearance and extends into the distal appendicular skeleton. Intense calvarial uptake that is disproportionate to that in the remainder of the skeleton is another feature of a metabolic superscan (Fig 7) (12).

Metastatic disease occasionally manifests as a solitary abnormality, usually in the spine. Degenerative changes may also manifest as an isolated abnormality. Single photon emission computed tomography (SPECT) is useful for differentiating between these two pathologic conditions (13,14). SPECT "removes" unwanted activity around the region of interest, thereby improving image contrast and allowing more precise lesion localization. This technique is particularly useful in the evaluation of anatomically complex structures such as the spine. With SPECT, sections of the vertebra can be examined on transaxial, coronal, sagittal, and three-dimensional images, which facilitates both localization and characterization of an abnormality (15).

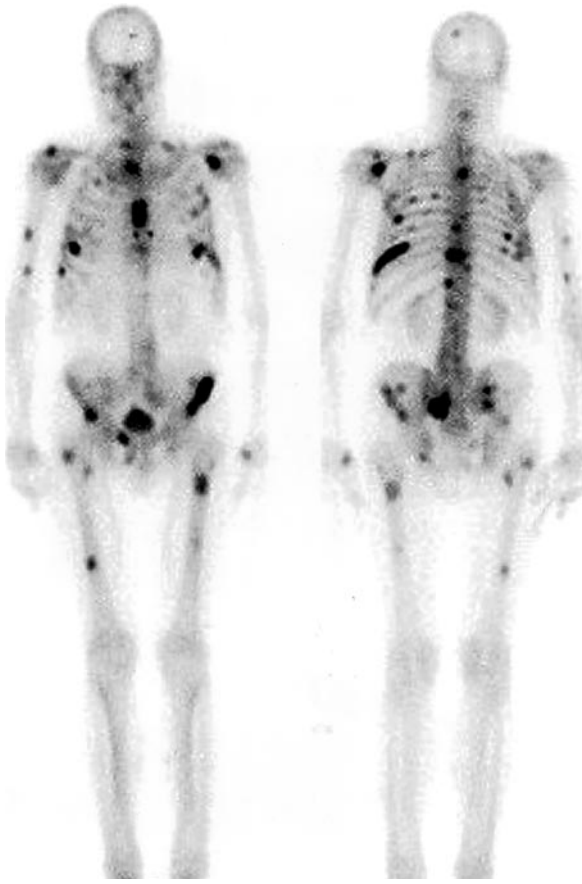

Figure 4. Extensive osseous metastases from lung carcinoma. Anterior (left) and posterior (right) whole-body bone scintigrams show multiple, randomly distributed foci of abnormal radiotracer uptake. The foci vary in size and intensity.

Abnormalities that extend beyond the vertebral body are invariably due to osteophytes, whereas abnormalities that are confined to the articular facets are nearly always benign in origin. Radiotracer accumulation in both the vertebral body and pedicles usually indicates metastatic disease, whereas abnormalities that involve the vertebral body and facets but spare the pedicles are usually benign (Figs 8, 9). Activity that is confined to the vertebral body can be due to tumor, trauma, or infection (13–15).

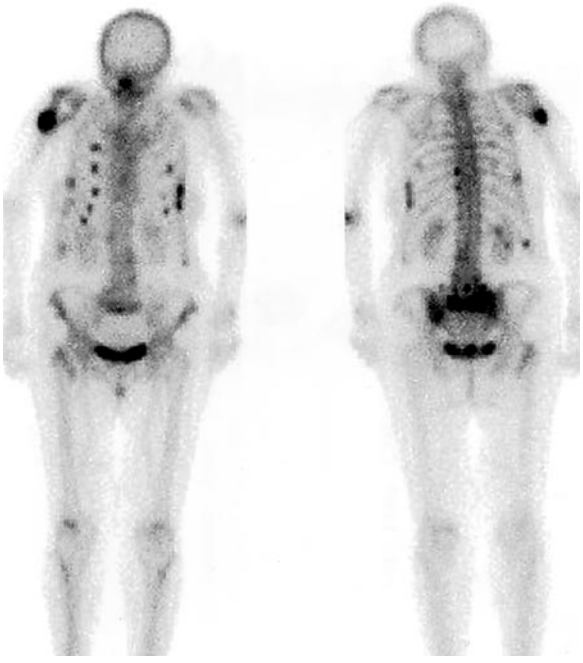

Figure 5. Anterior (left) and posterior (right) whole-body scintigrams obtained in a patient who fell demonstrate multiple foci of increased radiotracer uptake. The linearly distributed rib foci and H-shaped sacral activity indicate trauma as the cause of these foci. The increased activity in the right proximal humerus is due to a fracture.

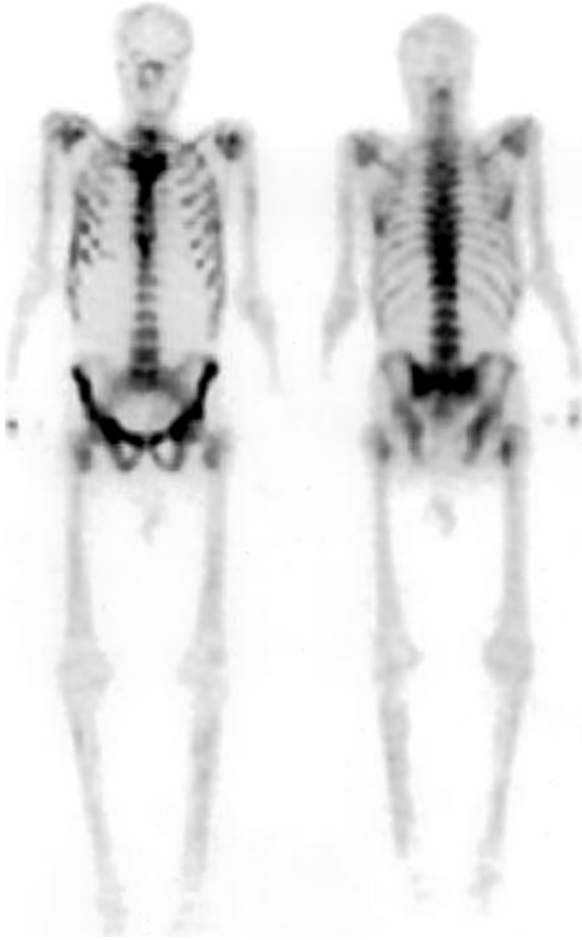

Figure 6. Bone metastases from gastric carcinoma. Anterior (left) and posterior (right) whole-body scintigrams show diffuse, irregularly increased activity throughout the appendicular and axial skeleton. There is minimal soft-tissue activity and virtually no renal or bladder activity. This pattern is indicative of diffuse bone metastases and is often referred to as a superscan.

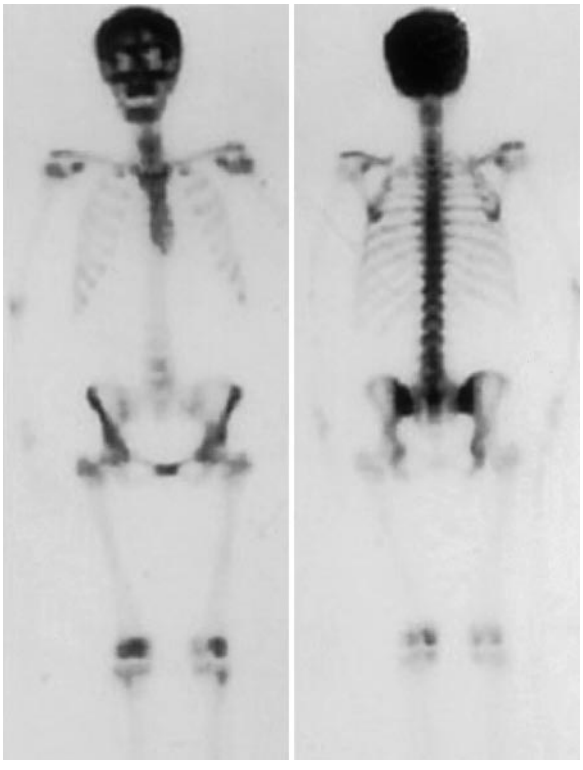

Figure 7. Renal osteodystrophy and secondary hyperparathyroidism. Anterior (left) and posterior (right) whole-body scintigrams demonstrate uniformly increased activity throughout the skeleton that is especially intense in the calvaria. These images show the superscan pattern associated with metabolic bone disease (cf Fig 6).

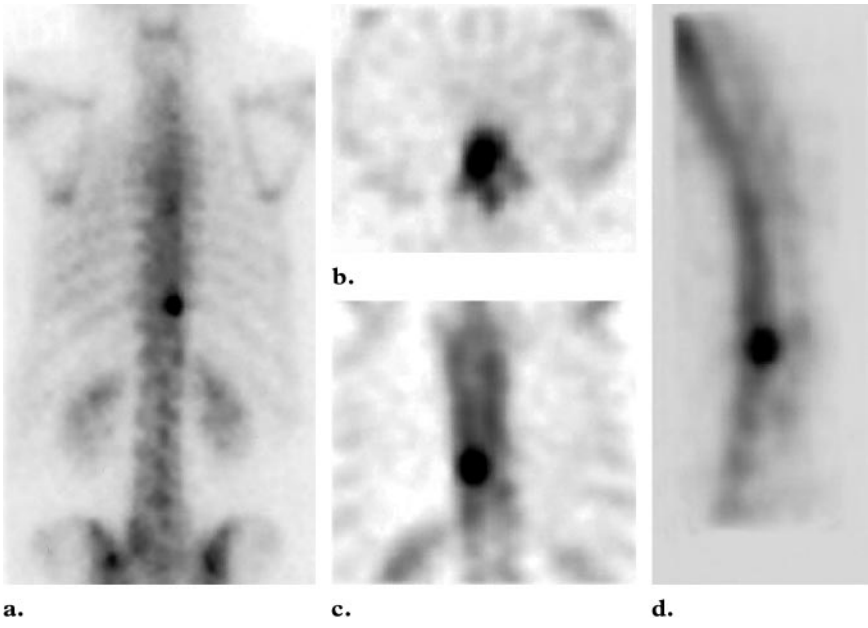

Figure 8. **(a)** Posterior planar scintigram demonstrates a focus of increased radiotracer uptake in the right side of a lower thoracic vertebra. **(b–d)** Transaxial **(b)**, coronal **(c)**, and sagittal **(d)** tomograms demonstrate that this eccentric activity extends from the body of the vertebra into the pedicle, a pattern that is consistent with metastatic disease.

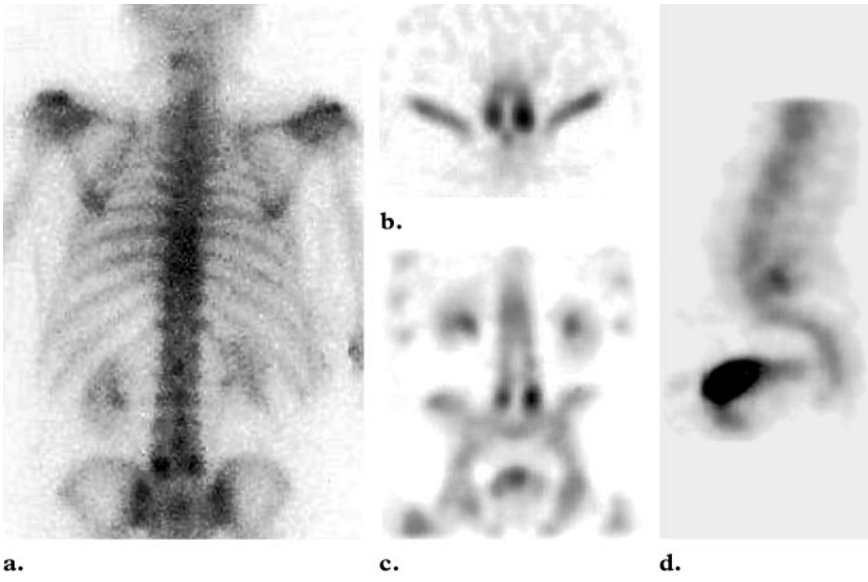

Figure 9. **(a)** Posterior planar scintigram shows bilateral foci of increased activity in a lower lumbar vertebra. **(b–d)** Transaxial **(b)**, coronal **(c)**, and sagittal **(d)** tomograms help confirm that this increased activity is confined to the posterior elements, sparing the pedicles, and therefore does not represent metastatic disease.

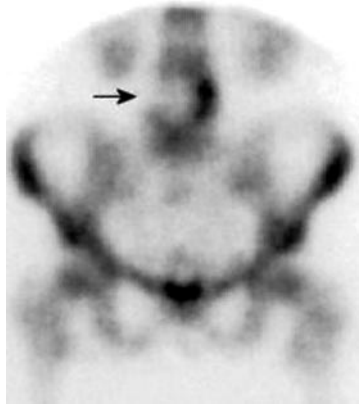

Figure 10. Scintigram shows a bone metastasis in a lower lumbar vertebra (arrow) as an area of decreased rather than increased activity.

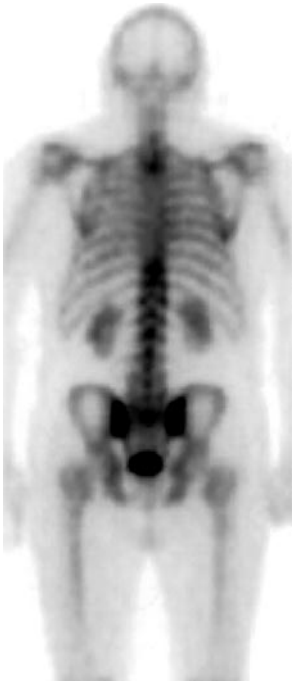

Figure 11. Posterior whole-body scintigram obtained about 1 year after mediastinal radiation therapy shows a sharply demarcated area of uniformly decreased radiotracer accumulation in the upper thoracic spine, a finding that represents the radiation port.

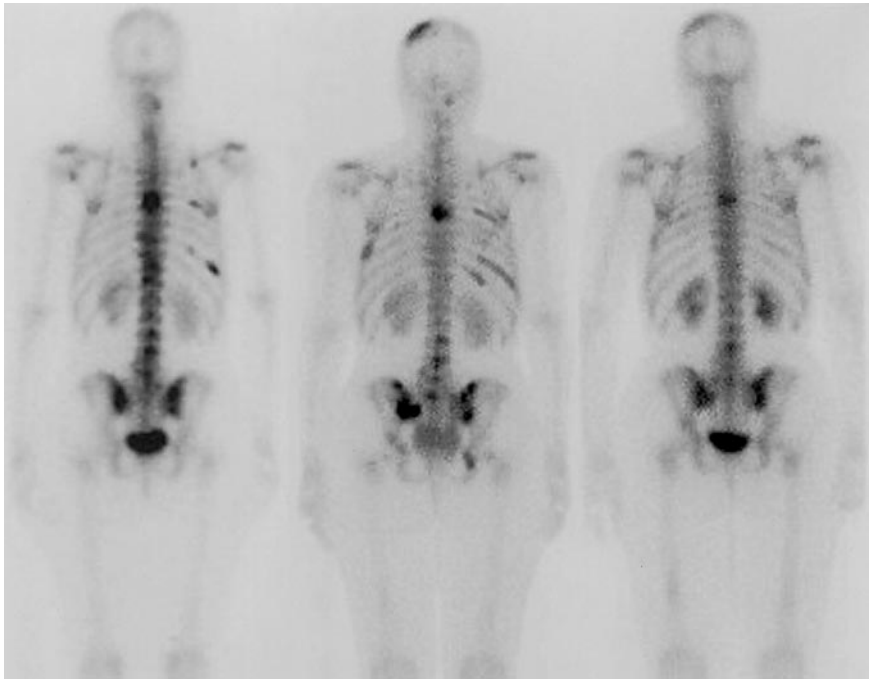

Figure 12. Bone metastasis from breast carcinoma. Scintigram from the initial bone study (left) demonstrates numerous foci of increased activity. On a scintigram obtained 3 months later (center), the abnormalities are more intense, and new abnormalities have become evident. On a third scintigram obtained yet 3 months later (right), many lesions have resolved, and those that remain have decreased in intensity. No new abnormalities have appeared. The changes present on the second study (center) reflect a response to treatment and the flare phenomenon, not disease progression.

SPECT acquisition parameters vary depending on whether a single-, dual-, or triple-head device is used. At our institution, 128 angular samplings (20 sec/sample) are acquired on a 128 × 128 × 16 matrix when a dual-head system is used. When a single-head system is used, 64 angular samplings (20 sec/sample) are acquired on a 128 × 128 × 16 matrix. Optimal reconstruction algorithms vary among manufacturers.

Although metastatic disease generally manifests as areas of increased activity, it can occasionally manifest as areas of decreased activity (Fig 10) (3). Other conditions that may manifest as focally decreased activity include acute-phase avascular necrosis and even osteomyelitis (16).

To accurately interpret radionuclide bone images obtained in patients with tumor, one must be cognizant of the effects that treatment can have on the study.

Many tumors are treated with radiation therapy. In the acute (early) phase of radiation osteitis, radiotracer uptake actually increases in the irradiated field as a result of inflammatory hyperemia (17). This increment, which peaks about 2–3 months after treatment, is only about 10%–20% above baseline and may not be appreciated at visual inspection of the images. The late phase of radiation osteitis is characterized by uniformly decreased uptake within the radiation port (Fig 11). This pattern, which can be identified by 6 months after treatment, is usually permanent, although on occasion, osseous uptake may return to pretreatment levels (3). The effects of radiation osteitis are usually seen only when doses of at least 17.5 Gy (1,750 rads) are administered (18).

Hormonal therapy and chemotherapy may also affect bone scan findings (17). An increase in intensity or the appearance of new abnormalities from one bone scan to the next does not necessarily indicate progression of disease. This pattern, seen in patients who are responding to treatment, reflects healing of the bone lesions and has been described as the "flare" phenomenon. This phenomenon is usually observed within 3 months after initiation of treatment and is often associated radiographically with the sclerotic changes that indicate healing. Continued increase in the number and intensity of lesions beyond 6 months is usually indicative of disease progression (19, 20). Serial studies over time are useful for differentiating healing from disease progression (Fig 12).

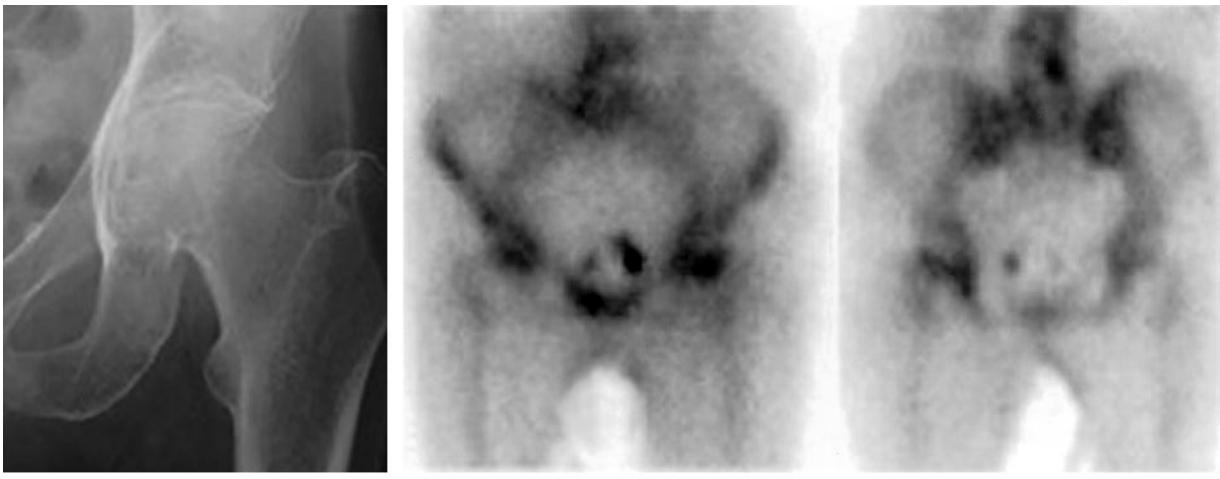

a. b.

c.

Figure 13. Fracture of the femur in an 83-year-old patient who complained of left hip pain after a fall. **(a)** Radiograph demonstrates normal findings. **(b)** Anterior (left) and posterior (right) radionuclide bone scans demonstrate foci of increased activity in the left femoral neck, a finding that is consistent with trauma. **(c)** Computed tomographic (CT) scan helps confirm the presence of a left femoral neck fracture (arrow).

Trauma

Although most fractures are detected radiographically, bone scintigraphy is useful for detecting fractures in patients with a history of trauma and equivocal or frankly negative radiographs (Fig 13). Most fractures are scintigraphically detectable within 24 hours of their occurrence; however, in elderly patients with osteopenia and unremarkable findings at initial bone scintigraphy performed within 24 hours of injury, repeat scintigraphy may be performed at 72 hours to maximize sensitivity. The minimum time for normalization of activity is 6 months after the fracture, and nearly all fractures will show normalization of activity by 2 years. Because remodeling is an ongoing process in nonaligned fractures, these fractures may never attain a normal scintigraphic appearance (21).

In athletic individuals, the lower extremity is often the site of musculoskeletal trauma. Commonly seen conditions include enthesopathies, stress fractures, and "shin splints" (22). Plantar fasciitis, a form of localized reactive periostitis, develops in individuals engaged in activities that involve extensive foot dorsiflexion, such as running and aerobics. Pain and tenderness are concentrated at the site of the insertion of the long plantar tendon into the inferior aspect of the calcaneus. The typical appearance of this entity on radionuclide bone images is that of focally increased activity, which may be intense, at the site of the tendon insertion (Fig 14) (22–24).

Radionuclide bone imaging is often used to differentiate tibial stress fractures from shin splints (Fig 15). Hyperperfusion and hyperemia are typically present in acute stress fracture. Delayed images demonstrate focal fusiform uptake in the lesion; this uptake often occurs at the junction of the middle and distal thirds of the tibia (25). Shin splints are due to excessive exertion of the tibialis and soleus muscles of the legs, which gives rise to periostitis at the tibial insertions of these muscles. Unlike in stress fractures, angiograms and blood pool images are usually normal in shin splints. Delayed bone images reveal longitudinally oriented linear areas of increased uptake of varying intensity that involve one-third or more of the posterior tibial cortex (26). The differentiation of stress fracture from shin splints is important because their treatments are very different.

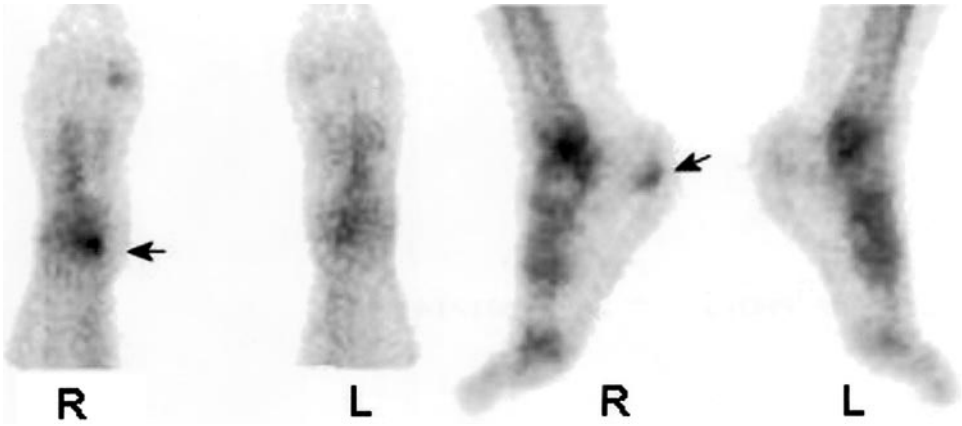

Figure 14. Plantar fasciitis. Radionuclide scans demonstrate foci of increased activity on the plantar surface of the right calcaneus (arrow), where the plantar fascia attaches to the calcaneal tuberosity.

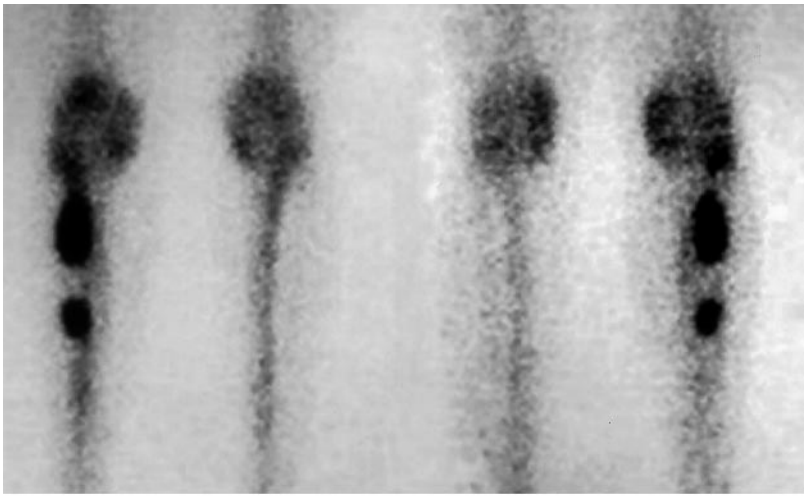

a.

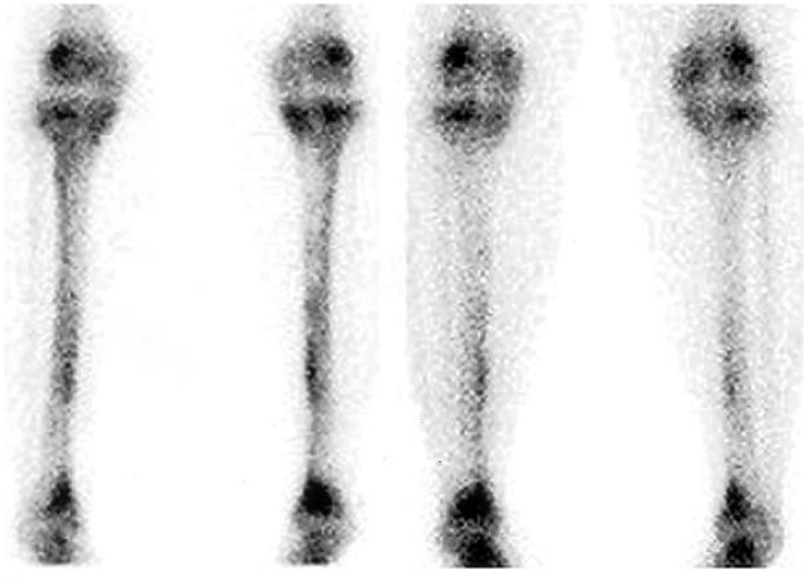

b.

Figure 15. **(a)** Anterior (left) and posterior (right) scintigrams obtained in a young woman with stress fractures of the right tibia show focal, intense activity in the proximal portion of the bone. (Case courtesy of Lawrence Davis, MD, Department of Radiology, Long Island Jewish Hospital, New Hyde Park, NY.) **(b)** On anterior (left) and posterior (right) scintigrams obtained in a patient with bilateral shin splints, the tibial activity is linear, longitudinally oriented, and mild in intensity.

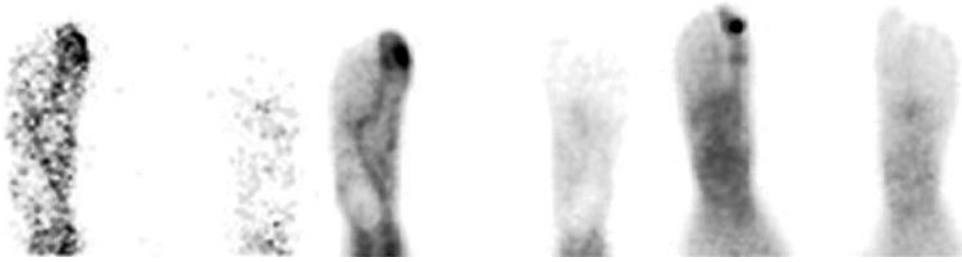

Figure 16. Osteomyelitis. Dynamic (left), blood pool (center), and bone (right) images from a three-phase bone scan demonstrate focal hyperperfusion, focal hyperemia, and foci of increased bone uptake, respectively, in the right great toe.

Infection

Three-phase bone scanning has an accuracy of over 90% and is the radionuclide procedure of choice for diagnosing osteomyelitis in bone not affected by underlying conditions (27).

The first (dynamic) phase reflects the relative amount of blood flow to the area of interest, whereas the second (blood pool) phase reflects the amount of activity that has extravasated into the tissues around the area of interest. The third (delayed [bone]) phase reflects the rate of bone turnover. The classic appearance of osteomyelitis on three-phase bone scans consists of focal hyperperfusion, focal hyperemia, and focally increased bone uptake (Fig 16). Abnormalities at radionuclide bone imaging reflect increased bone mineral turnover in general, not infection specifically. Therefore, conditions associated with increased bone mineral turnover (eg, tumors, fractures, joint neuropathy) may mimic osteomyelitis at three-phase bone scintigraphy. Under these circumstances, three-phase bone imaging is less useful, primarily because of diminished specificity. To improve specificity, complementary imaging with gallium-67 citrate (for spinal infection) or indium-111–labeled autologous leukocytes (for the appendicular skeleton) is often performed (27).

Bone scintigraphy is often used to evaluate painful joint replacement. A negative study is strong evidence that the prosthesis is not the source of the patient's discomfort. However, the significance of increased periprosthetic uptake is less certain. Factors that must be taken into account include the type and location of the prosthesis and the amount of time elapsed between implantation and imaging (28).

Miscellaneous Conditions

Paget Disease

Paget disease, a focal disorder of skeletal metabolism of unknown cause, is characterized by increased resorption, disordered remodeling, and nonuniform mineralization of bone (29). Affected bones become enlarged, irregular, and deformed. At scintigraphy, these changes manifest as intensely increased activity throughout the involved bones (Fig 17) (30). The one exception to this pattern is osteoporosis circumscripta, in which intense activity is confined to the margins of the lesion (31).

Hypertrophic Osteoarthropathy

Hypertrophic osteoarthropathy is secondary to cortical periostitis that arises in connection with various intrathoracic tumors, pulmonary diseases, cardiac conditions, and intraabdominal diseases (17). It is believed that an as yet unidentified cytokine exerts an osteogenic effect (32). The most common scintigraphic pattern is nonuniform, irregular cortical uptake involving the long bones and giving rise to the "tramline sign" (Fig 18) (33).

Reflex Sympathetic Dystrophy

Reflex sympathetic dystrophy, a syndrome that causes significant discomfort, is thought to be due to "sympathetic overflow," which may explain the pain, warmth, and swelling of the involved extremity (34). At bone scintigraphy, reflex sympathetic dystrophy usually manifests as diffuse, uniformly increased uptake throughout the affected region (Fig 19). Occasionally, reflex sympathetic dystrophy may manifest as a focal abnormality limited to, for example, the hand or knee. Decreased radiotracer accumulation has also been described, especially in children (34–37).

Figure 17. Paget disease. Whole-body scintigram demonstrates increased radiotracer accumulation in the proximal right femur and in the deformed and enlarged tibias.

Figure 18. Lung carcinoma with hypertrophic osteoarthropathy. Anterior (left) and posterior (right) whole-body scintigrams demonstrate pericortical stripes of activity (tramline sign) in the lower extremities. Hypertrophic osteoarthropathy is also present in the bones of the forearms.

Figure 19. Reflex sympathetic dystrophy. Scintigram shows diffusely increased uptake in the distal right upper extremity.

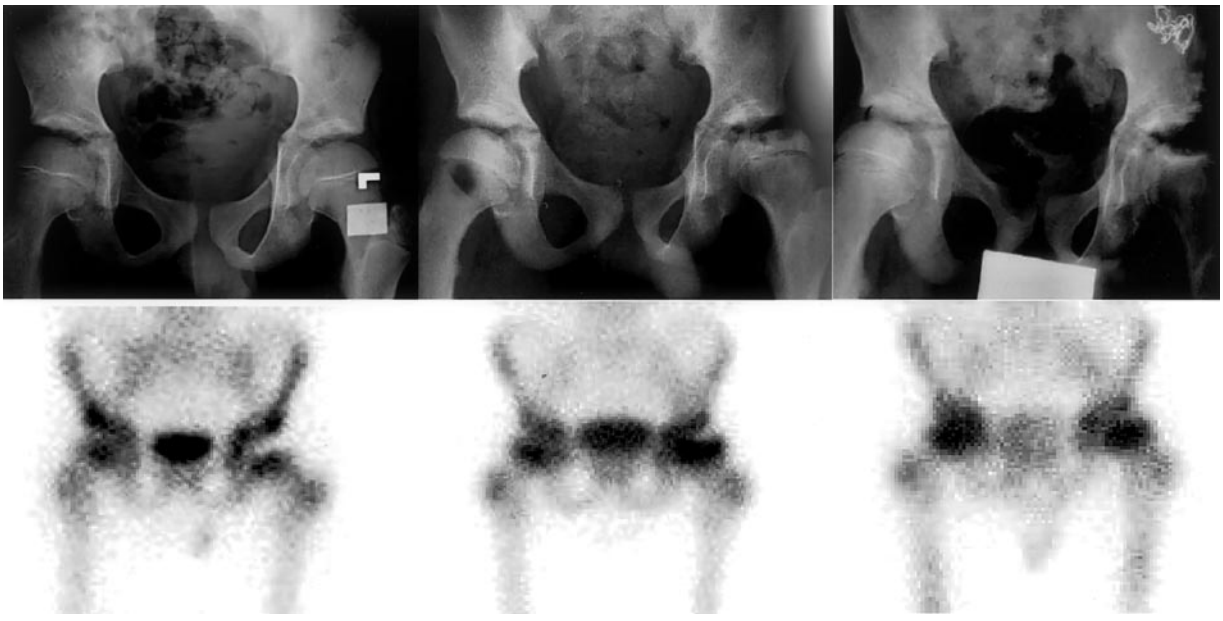

Figure 20. Avascular necrosis in a patient with sickle cell disease who complained of left hip pain. Radiograph from an initial study (top left) shows normal findings. The corresponding scintigram (bottom left) demonstrates an abnormality with a photopenic defect in the left femoral head. Radiograph obtained 1 year later (top center) shows deformity of the left femoral head. The corresponding scintigram (bottom center) reveals increased radiotracer uptake, a finding that represents the reparative phase of avascular necrosis. Radiograph obtained 2 years after the initial study (top right) shows evidence of progressive destruction and deformity of the left femoral head. The corresponding scintigram (bottom right) depicts a small, deformed left femoral head.

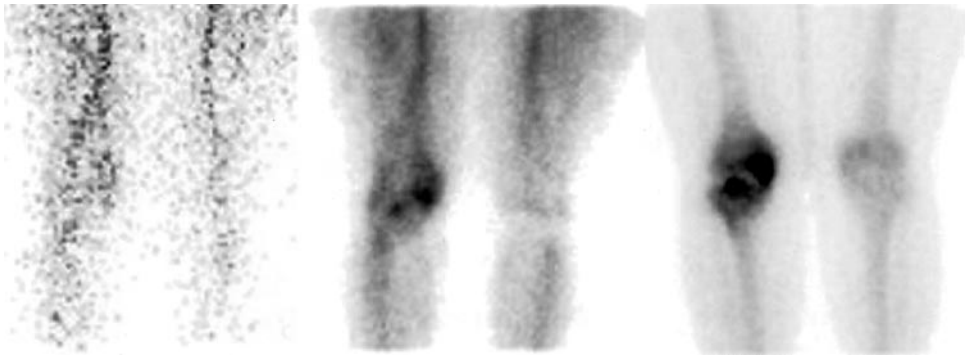

Figure 21. Spontaneous osteonecrosis. Dynamic (left), blood pool (center), and bone (right) images show focal hyperperfusion, hyperemia, and bone activity, respectively, in the intercondylar region of the tibia and medial femoral condyle.

Avascular Necrosis

Disruption of arterial supply to or obstruction of venous outflow from an enclosed joint such as the hip results in oxygen deprivation, which leads to the death of osteocytes. Vascular insufficiency for as little as 12 hours can cause osteonecrosis. In the acute phase of vascular compromise, no radiotracer is delivered to the bone tissue. At scintigraphy, the affected part of the bone appears as a photopenic defect. After revascularization, exuberant osteoblastic repair manifests as intense radiotracer uptake. Subsequently, when repair is complete, radiotracer uptake may return to baseline levels (Fig 20) (37). Spontaneous osteonecrosis may occur in elderly individuals, especially women, and is characterized by a sudden onset of

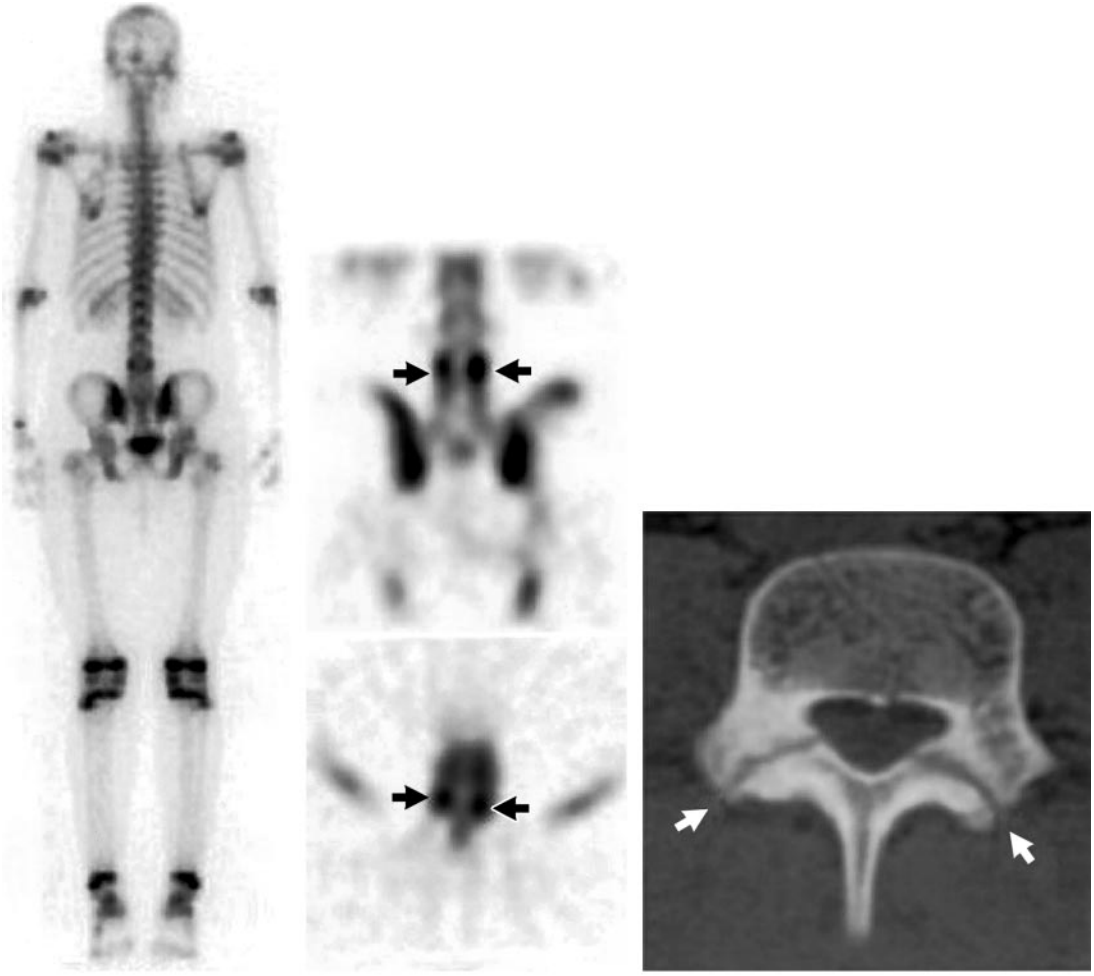

a. b. c.

Figure 22. Bilateral spondylolysis. **(a)** Posterior whole-body scintigram shows minimally increased activity in the lower lumbar spine. **(b)** Coronal (top) and transverse (bottom) SPECT images clearly show bilateral foci of intense activity in the posterior elements of L4 (arrows). **(c)** CT scan helps confirm the presence of bilateral spondylolysis (arrows).

knee pain with normal radiographic findings. At scintigraphy, spontaneous osteonecrosis is characterized by focally increased radiotracer accumulation, usually in the medial femoral condyle, although the lateral femoral condyle and tibia may also be involved (Fig 21) (38). Radionuclide imaging is superior to conventional radiography in the detection of avascular necrosis but is less sensitive than magnetic resonance imaging, which is currently the preferred imaging technique in this setting (39).

Spondylolysis

Spondylolysis, a condition caused by a defect in the pars interarticularis of a vertebra, is an important cause of pain in active young adults. When initial radiographs are negative, bone scintigraphy may serve to initiate more specialized anatomic imaging for diagnosis. In addition to planar imaging, SPECT of the thoracolumbar spine is mandatory to ensure adequate examination (Fig 22) (36).

Venous Obstruction

Patients with venous obstruction often present with swelling and edema of the affected area. On dynamic-phase images from a three-phase bone study, collateral vessels may be identified (Fig 23).

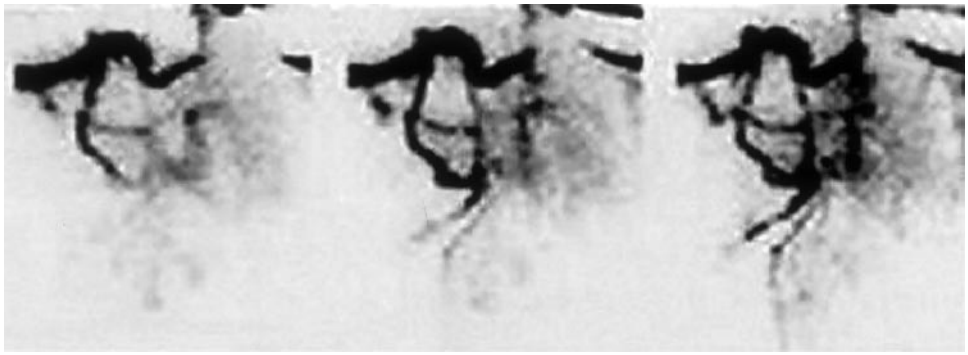

Figure 23. Lung carcinoma with superior vena caval obstruction. Dynamic-phase radionuclide images obtained 3 (left), 6 (center), and 9 (right) seconds after injection show dilated major vessels and collateral vessels.

Figure 24. Myocardial uptake in a patient with long-standing congestive heart failure. Whole-body scintigram shows myocardial uptake and abdominal ascites.

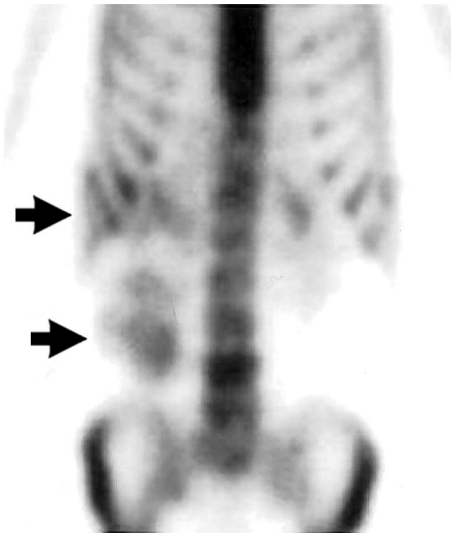

Figure 25. Hepatic metastasis from colon carcinoma. Scintigram shows areas of increased radiotracer uptake (arrows), findings that represent metastases to the liver.

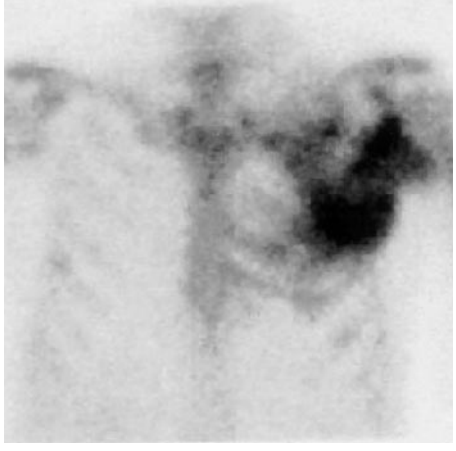

Figure 26. Rhabdomyolysis. Scintigram shows intense skeletal muscle uptake in the anterior portion of the left upper thorax.

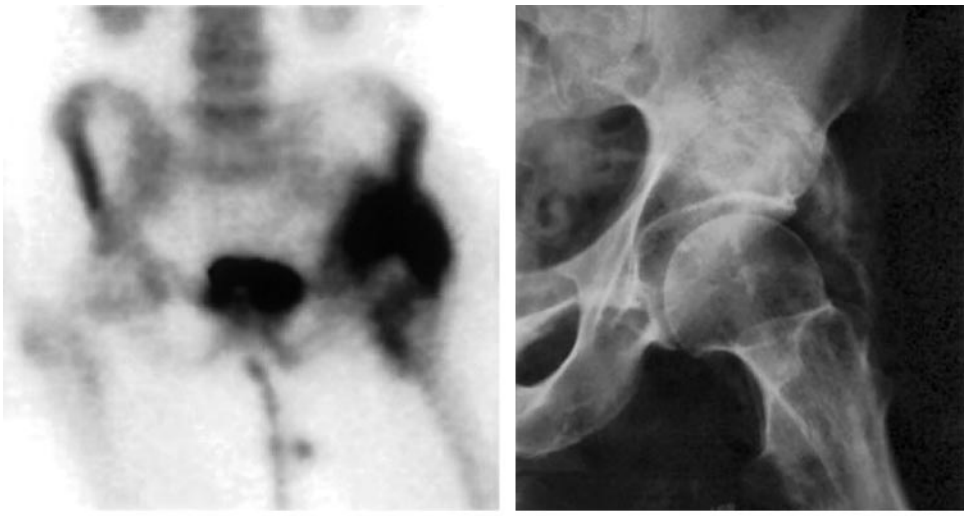

a. b.

Figure 27. Heterotopic ossification in a patient with a history of fracture of the left hip. **(a)** Scintigram shows intense radiotracer activity around the left hip. **(b)** Radiograph helps confirm the presence of heterotopic ossification.

Figure 28. Autoinfarcted spleen in a patient with sickle cell disease. Posterior scintigram shows left suprarenal activity in the spleen (arrow).

Extraosseous Activity

Soft-tissue uptake of diphosphonates can be seen in many pathologic conditions. Although the causes of such uptake are multifactorial, one important factor is the formation of calcium phosphate salts from calcium and phosphate that leak into the extracellular fluid from hypoxic or dead cells. These salts bind to the diphosphonates (40). Recognition of extraosseous uptake of diphosphonates has practical diagnostic implications and may at times point to a systemic disease.

Myocardial uptake has been described in longstanding congestive heart failure, myocardial infarction, pericarditis, amyloidosis, unstable angina, and postresuscitation or cardioversion (Fig 24) (41). Metastases to various anatomic structures such as the liver and lymph nodes demonstrate accumulation of radiotracer from bone (Fig 25). Sarcolemmal disruption in calcium-rich skeletal muscle likely explains the accumulation of diphosphonates in rhabdomyolysis (Fig 26) (41,42). Heterotopic ossification, which is due to the presence of extraskeletal osteoblastic cells, occurs in patients with fractures, joint replacements, paraplegia, and poststroke hemiplegia (Fig 27) (43). An autoinfarcted spleen, which is common in patients with sickle cell disease, appears as a focus of activity superolateral to the left kidney (Fig 28) (44).

Extraosseous uptake may also result from the introduction of air into the vial or syringe containing Tc-99m–labeled diphosphonates. The air

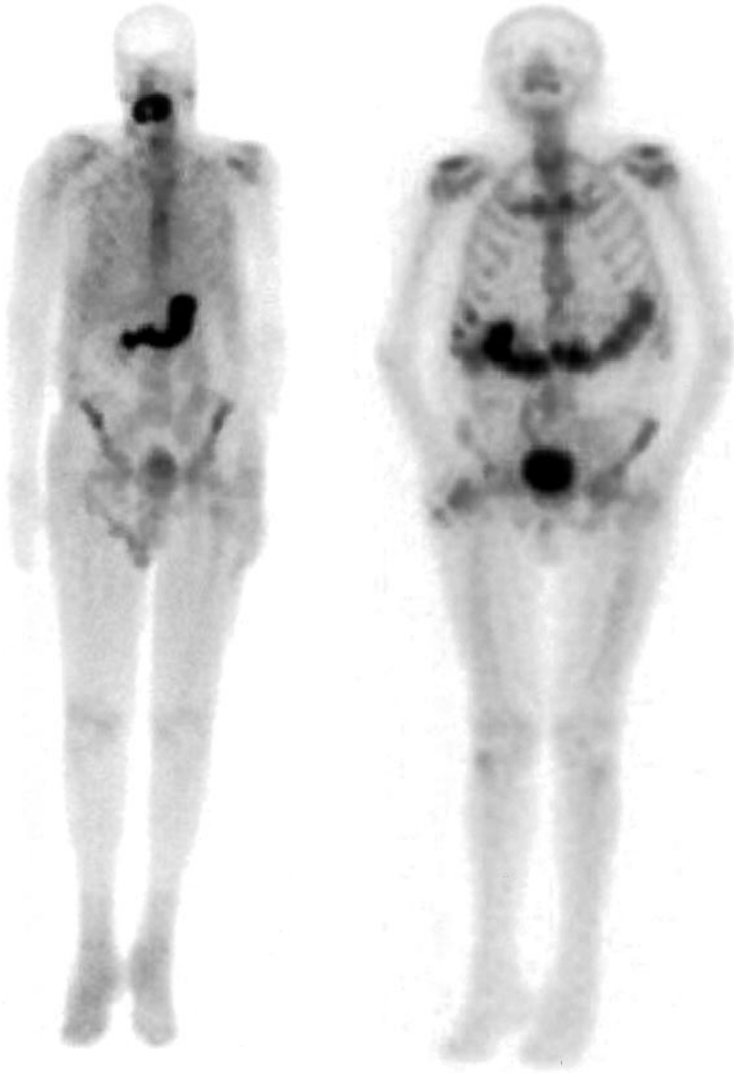

Figure 29. Extraosseous uptake. Anterior whole-body scintigram demonstrates poor bone detail and intense oral and gastric activity. These findings are caused by the introduction of air into the vial or syringe containing the radiotracer, which results in oxidation of the compound and the liberation of free pertechnetate.

causes oxidation and breakdown of the radiolabeled compound with release of free pertechnetate. The findings of oral, thyroid, and gastric activity on a radionuclide bone image are confirmatory (Fig 29) (10). Sometimes extraosseous activity represents residual activity from a previous radionuclide procedure; thus, the importance of obtaining a thorough history cannot be overemphasized (Fig 30).

Artifacts

Spurious abnormalities may be produced by jewelry, articles of clothing, and even medical devices (Fig 31) (3).

Figure 30. Extraosseous uptake. Anterior whole-body scintigram demonstrates colonic activity due to previous myocardial perfusion imaging with Tc-99m sestamibi.

Conclusions

Bone scintigraphy is a popular and important imaging modality and will likely remain so for the foreseeable future. Although bone scintigraphy is not specific, its exquisite sensitivity makes it a useful screening procedure for many pathologic conditions. Moreover, some conditions that are not evident on anatomic images can be diagnosed with radionuclide bone imaging.

References

1. Genant HK, Bautovich GJ, Singh M, Lathrop KA, Harper PV. Bone-seeking radionuclides: an in vivo study of factors affecting skeletal uptake. Radiology 1974; 113:373–382.

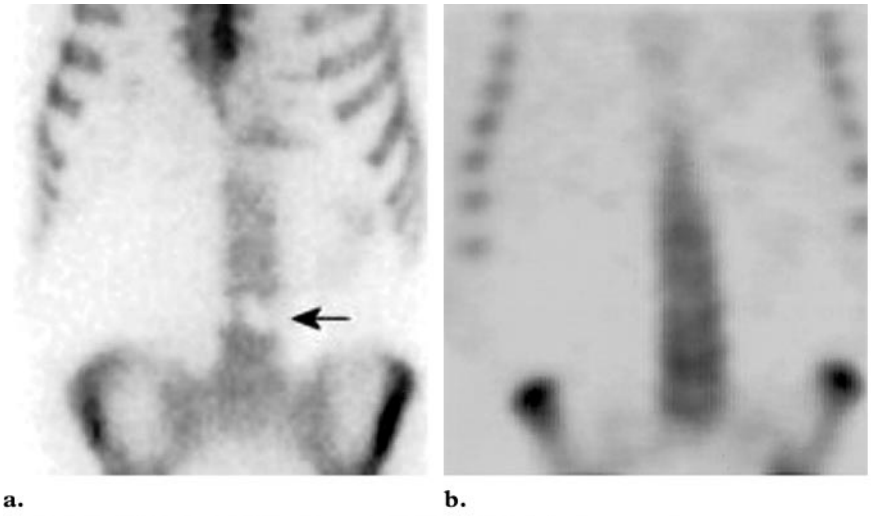

Figure 31. Artifact from an implanted defibrillator. **(a)** Planar scintigram shows an apparent photopenic defect in the lower lumbar spine (arrow). **(b)** Coronal SPECT image does not demonstrate any bone abnormality. **(c)** Scout CT scan reveals that the cause of the defect is an implanted defibrillator. **(d)** Transaxial CT scan shows the defibrillator in the left anterior abdominal wall (arrow).

2. Galasko CSB. The pathological basis for skeletal scintigraphy. J Bone Joint Surg Br 1975; 57:353–359.
3. McAfee JG, Reba RC, Majd M. The musculoskeletal system. In: Wagner HN Jr, Szabo Z, Buchanan JW, eds. Principles of nuclear medicine. 2nd ed. Philadelphia, Pa: Saunders, 1995; 986–1012.
4. Citrin DL, Tormey DC, Carbone PP. Implications of the 99mTc diphosphonate bone scan on treatment of primary breast cancer. Cancer Treat Rep 1977; 61:1249–1252.
5. Fon GT, Wong WS, Gold RH, Kaiser LR. Skeletal metastases of melanoma: radiographic, scintigraphic, and clinical review. AJR Am J Roentgenol 1981; 137:103–108.
6. Galasko CS, Doyle FH. The detection of skeletal metastases from mammary cancer: a regional comparison between radiology and scintigraphy. Clin Radiol 1972; 23:295–297.
7. Hage WD, Aboulafia AJ, Aboulafia DM. Incidence, location, and diagnostic evaluation of metastatic bone disease. Orthop Clin North Am 2000; 31:515–528.
8. Palmer E, Henrikson B, McKusick K, Strauss HW, Hochberg F. Pain as an indicator of bone metastasis. Acta Radiol 1988; 29:445–449.
9. Bibbo C, Patel DV, Benevenia J. Perioperative considerations in patients with metastatic bone disease. Orthop Clin North Am 2000; 31:577–595.
10. Thrall JH, Ziessman HA. Skeletal system. In: Thrall JH, Ziessman HA, eds. Nuclear medicine: the requisites. 2nd ed. St Louis, Mo: Mosby, 2001; 110–144.
11. Weckesser M, Muller-Mattheis VG, Vosberg H, Muller-Gartner HW. Pathogenetic differentiation

of the bone superscan using bone marrow scintigraphy. Nuklearmedizin 1998; 37:156–158. [German]
12. Mari C, Catafau A, Carrio I. Bone scintigraphy and metabolic disorders. Q J Nucl Med 1999; 43: 259–267.
13. Savelli G, Maffioli L, Maccauro M, De Deckere E, Bombardieri E. Bone scintigraphy and the added value of SPECT (single photon emission tomography) in detecting skeletal lesions. Q J Nucl Med 2001; 45:27–37.
14. Even-Sapir E, Martin RH, Barnes DC, Pringle CR, Iles SE, Mitchell MJ. Role of SPECT in differentiating malignant from benign lesions in the lower thoracic and lumbar vertebrae. Radiology 1993; 187:193–198.
15. Delpassand ES, Garcia JR, Bhadkamkar V, Podoloff DA. Value of SPECT imaging of the thoracolumbar spine in cancer patients. Clin Nucl Med 1995; 20:1047–1051.
16. Pennington WT, Mott MP, Thometz JG, Sty JR, Metz D. Photopenic bone scan osteomyelitis: a clinical perspective. J Pediatr Orthop 1999; 19: 695–698.
17. Stokkel MPM, Valdes Olmos RA, Hoefnagel CA, Richel DJ. Tumor and therapy associated abnormal changes on bone scintigraphy: old and new phenomena. Clin Nucl Med 1993; 18:821–828.
18. King MA, Weber DA, Casarett GW, Burgener FA, Corriveau O. A study of irradiated bone. II. Changes in Tc-99m pyrophosphate bone imaging. J Nucl Med 1980; 21:22–30.
19. Coombes RC, Dady P, Parsons C, et al. Assessment of response of bone metastases to systemic treatment in patients with breast cancer. Cancer 1983; 52:610–614.
20. Coleman RE, Mashiter G, Whitaker KB, Moss DW, Rubens RD, Fogelman I. Bone scan flare predicts successful systemic therapy for bone metastases. J Nucl Med 1988; 29:1354–1359.
21. Matin P. The appearance of bone scans following fractures, including immediate and long-term studies. J Nucl Med 1979; 20:1227–1231.
22. Murray IPC. Bone scintigraphy in trauma. In: Murray IPC, Ell PJ, eds. Nuclear medicine in clinical diagnosis and treatment. 2nd ed. Edinburgh, Scotland: Churchill Livingstone, 1998; 1241–1267.
23. Aburano T, Yokoyama K, Taki J, Nakajima K, Tonami N, Hisada K. Tc-99m MDP bone imaging in inflammatory enthesopathy. Clin Nucl Med 1990; 15:105–106.
24. Intenzo CM, Wapner KL, Park CH, Kim SM. Evaluation of plantar fasciitis by three-phase bone scintigraphy. Clin Nucl Med 1991; 16:325–328.
25. Rupani HD, Holder LE, Espinola DA, Engin SI. Three-phase radionuclide bone imaging in sports medicine. Radiology 1985; 156:187–196.
26. Holder LE, Michael RH. The specific scintigraphic pattern of "shin splints in the lower leg": concise communication. J Nucl Med 1984; 25: 865–869.
27. Palestro CJ, Torres MA. Radionuclide imaging of orthopedic infections. Semin Nucl Med 1997; 27: 334–345.
28. Love C, Tomas MB, Marwin SE, Pugliese PV, Palestro CJ. Role of nuclear medicine in diagnosis of the infected joint replacement. RadioGraphics 2001; 21:1229–1238.
29. Kanis JA. Paget's disease of bone (osteitis deformans). In: Goldman L, Bennett JC, eds. Cecil textbook of medicine. 21st ed. Philadelphia, Pa: Saunders, 2000; 1413–1416.
30. Wellman HN, Schauwecker D, Robb JA, Khairi MR, Johnston CC. Skeletal scintimaging and radiography in the diagnosis and management of Paget's disease. Clin Orthop 1977; 127:55–62.
31. Rausch JM, Resnick D, Goergen TG, Taylor A. Bone scanning in osteolytic Paget's disease: case report. J Nucl Med 1977; 18:699–701.
32. Ernstoff MS, Meehan KR. Nonmetastatic effects of cancer: other systems. In: Goldman L, Bennett JC, eds. Cecil textbook of medicine. 21st ed. Philadelphia, Pa: Saunders, 2000; 1057–1059.
33. Ali A, Tetalman MR, Fordham EW, et al. Distribution of hypertrophic pulmonary osteoarthropathy. AJR Am J Roentgenol 1980; 134:771–780.
34. Fournier RS, Holder LE. Reflex sympathetic dystrophy: diagnostic controversies. Semin Nucl Med 1998; 28:116–123.
35. Kozin F, Soin JS, Ryan LM, Carrera GF, Wortmann RL. Bone scintigraphy in the reflex sympathetic dystrophy syndrome. Radiology 1981; 138: 437–443.
36. Nadel HR, Stilwell ME. Nuclear medicine topics in pediatric musculoskeletal disease: techniques and applications. Radiol Clin North Am 2001; 39:619–651.
37. Murray IPC. Vascular manifestations. In: Murray IPC, Ell PJ, eds. Nuclear medicine in clinical diagnosis and treatment. 2nd ed. Edinburgh, Scotland: Churchill Livingstone, 1998; 1223–1240.
38. Galasko CSB, Weber DA. Avascular necrosis. In: Galasko CSB, Weber DA, eds. Radionuclide scintigraphy in orthopaedics. Edinburgh, Scotland: Churchill Livingstone, 1984; 200–209.
39. DeSmet AA, Dalinka MK, Alazraki N, et al. Diagnostic imaging of avascular necrosis of the hip. Radiology 2000; 215(suppl):247–254.
40. Heck LL. Extraosseous localization of phosphate bone agents. Semin Nucl Med 1980; 10:311–313.
41. Silberstein EB, Elgazzar AH, Fernandez-Ulloa M, Nishiyama H. Skeletal scintigraphy in non-neoplastic osseous disorders. In: Henkin RE, Bloes MA, Dillehay GL, et al. Nuclear medicine. St Louis, Mo: Mosby, 1996; 1141–1197.
42. Blair RJ, Schroeder ET, McAfee JG, Duxbury CE. Skeletal muscle uptake of bone seeking agents in both traumatic and non-traumatic rhabdomyolysis with acute renal failure (abstr). J Nucl Med 1975; 16(P):515–516.
43. Buring K. On the origin of cells in heterotopic bone formation. Clin Orthop 1975; 110:293–302.
44. Silberstein EB, DeLong S, Cline J. Tc99m diphosphonate and sulfur colloid uptake by the spleen in sickle disease: interrelationship and clinical correlates: concise communication. J Nucl Med 1984; 25:1300–1303.